Early Stages in the Nucleation Process of Carbon Nanotubes

Matthieu Moors,[†] Hakim Amara,[‡] Thierry Visart de Bocarmé,[†] Christophe Bichara,[∥] François Ducastelle,[§] Norbert Kruse,[†,*] and Jean-Christophe Charlier[¶]

[†]Chemical Physics of Materials, Faculté des Sciences, Université Libre de Bruxelles, Campus Plaine, CP 243, 1050 Bruxelles, Belgium, [‡]Laboratoire Francis Perrin, CEA Saclay, Bâtiment 522, 91191 Gif sur Yvette Cedex, France, [§]Laboratoire d'Etudes des Microstructures, ONERA-CNRS, BP 72, 92322 Châtillon, France, [∥]CINaM, CNRS and Aix-Marseille Universities, Campus de Luminy, 13288 Marseille, France, and [¶]Unité de Physico-Chimie et de Physique des Matériaux (PCPM), European Theoretical Spectroscopy Facility (ETSF), Université Catholique de Louvain, Place Croix du Sud 1, 1348 Louvain-la Neuve, Belgium

ABSTRACT The early stages of carbon nanotube nucleation are investigated using field ion/electron microscopy along with *in situ* local chemical probing of a single nanosized nickel crystal. To go beyond experiments, *tight-binding* Monte Carlo simulations are performed on oriented Ni slabs. Real-time field electron imaging demonstrates a carbon-induced increase of the number density of steps in the truncated vertices of a polyhedral Ni nanoparticle. The necessary diffusion and step-site trapping of adsorbed carbon atoms are observed in the simulations and precede the nucleation of graphene-based sheets in these steps. Chemical probing of selected nanofacets of the Ni crystal reveals the occurrence of C_n ($n = 1-4$) surface species. Kinetic studies prove C_{2+} species are formed from C_1 with a delay time of several milliseconds at 623 K. Carbon dimers, C_2, must not necessarily be formed on the Ni surface. Tight-binding Monte Carlo simulations reveal the high stability of such dimers in the first layer beneath the surface.

KEYWORDS: carbon nanotubes · chemical vapor deposition · field ion microscopy · atom-probe · Monte Carlo simulations · tight-binding

Since the discovery of carbon nanotubes (CNTs), the scientific community has investigated the unique electrical, chemical, and mechanical properties of these highly versatile 1D materials from both fundamental and applied points of view.[1] Among the different syntheses, catalytic chemical vapor deposition (CVD) methods are versatile and offer the possibility of producing CNTs in large quantities.[1] However, nanotube science still suffers from a serious lack of detailed knowledge on the kinetics and microscopic growth mechanisms ruling their nucleation and, consequently, their synthesis. Truly atomistic approaches are mainly based on computer modeling using *ab initio* static calculations,[2−4] quantum molecular dynamics,[5−8] and force-field[9] and semiempirical techniques.[10] Most of these theoretical models rest upon the concepts of the most commonly accepted vapor−liquid−solid growth mechanism,[11] which has recently been challenged by *in situ* observations in the environmental transmission electron microscope (TEM).[4,12−16] Accordingly, the catalyst—most frequently Ni or Co nanosized particles on a support—remains solid and metallic (at least for Ni catalysts) during the growth process. Moreover, the occurrence of an incubation period[12] before the onset of sp^2 carbon growth has been observed experimentally but remains little understood at present. Scanning tunneling microscopy (STM) has demonstrated the high activity of step sites for the dissociation of carbon-containing gases (C_2H_4 and CO) on 2D oriented Ni single-crystal surfaces but has as yet failed to elucidate the local chemistry and reactivity of deposited carbon as a prerequisite to nanotube nucleation.[17,32] On the other hand, LEED (low energy electron diffraction) and STM have previously demonstrated the occurrence of well-defined carbon-induced reconstruction forms of densely packed Ni single-crystal surfaces at relatively low reaction temperatures.[18−22]

RESULTS AND DISCUSSION

In the present work, the early stages of CNT nucleation mechanisms are investigated through the combined application of *video*-field emission microscopy and *tight-binding* Monte Carlo (TBMC) simulations. Both the atomic structure and the chemical composition of a single nanosized Ni crystal are analyzed on the local scale of about 400 surface atoms during the ongoing interaction with acetylene at elevated temperatures (Figure 1a demonstrates the general principle of the atom-probe technique and the use of the Ni crystal as a nanoreactor). Carbon-induced formation of step sites is observed in real-time and suggested to be responsible for the

*Address correspondence to nkruse@ulb.ac.be.

Received for review November 14, 2008 and accepted February 06, 2009.

Published online February 16, 2009.
10.1021/nn800769w CCC: $40.75

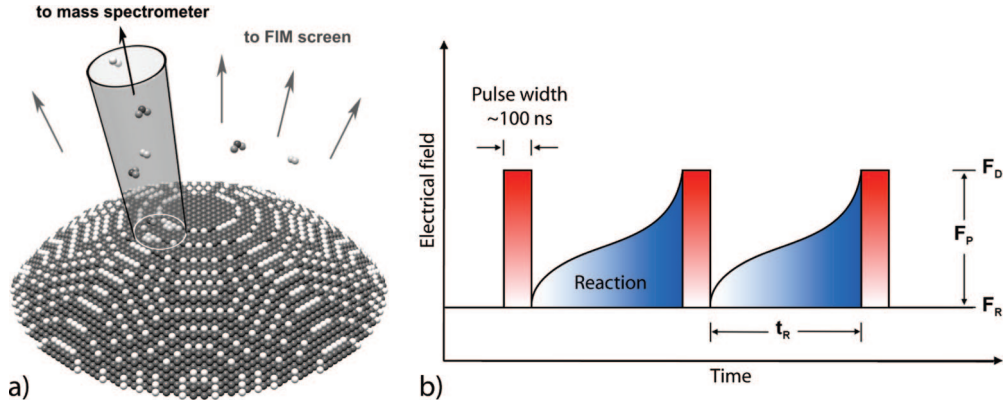

Figure 1. (a) Basic scheme of the 1D atom-probe technique applied during the ongoing reaction. Surface species are field-desorbed as ions from selected surface facets and injected into a time-of-flight mass spectrometer for chemical identification. (b) Application of short field pulses with well-defined frequency (between 10 kHz and 1 Hz at 100 ns pulse width). The total desorption field, F_D, is the sum of the steady field, F_R (which can be switched off for field-free reaction studies), and the pulsed field, F_P. Variation of the pulse repetition frequency (*i.e.*, the reaction time t_R) reveals the kinetics of the reaction process.

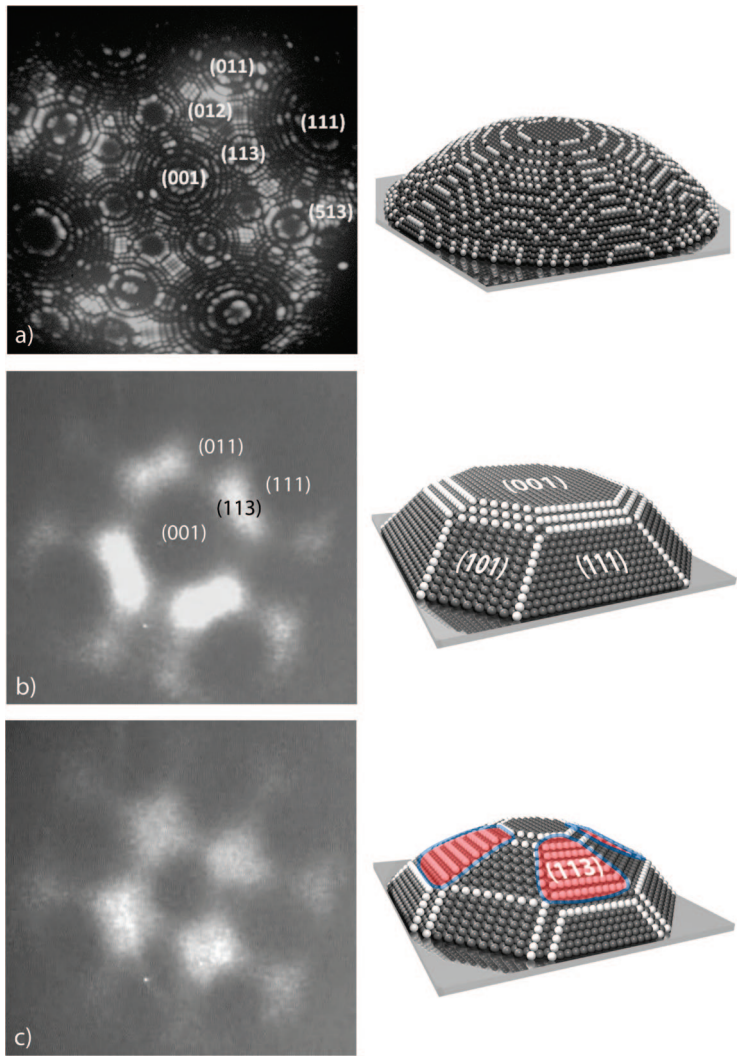

Figure 2. (a) Ne-FIM micrograph of the clean Ni crystal along with a corresponding ball model (T = 61 K, $F \sim$ 35 V/nm). (b) FEM micrograph of the same sample under H_2 atmosphere ($p = 10^{-4}$ Pa, T = 873 K) along with a ball model stressing its facetted shape. (c) FEM micrograph of the sample 11 s after acetylene introduction ($p_{tot} = 2.5 \times 10^{-4}$ Pa, T = 873 K) and corresponding ball model (red areas highlight the extended step containing crystal planes). Suggested models are 2.5 times smaller than the real crystal.

occurrence of the incubation time before carbon nanotube nucleation. Moreover, time-resolved studies (explained in the Methods section) demonstrate the dimerization to be rate-limiting in the polymerization of atomic surface carbon. Interestingly, the theoretical studies indicate such C_2 dimers are quite stable in the first layer beneath the Ni surface, meaning that the nucleation process involves surface and subsurface processes concurrently.

Starting from a clean and well-characterized crystal (Figure 2a), a first set of experiments is designed to reveal the Ni sample geometry at 873 K under a hydrogen flow at 10^{-4} Pa. This procedure mimics the CVD process since catalyst preconditioning with reducing gases such as H_2 or NH_3 generally precedes CNT synthesis. As illustrated in Figure 2b, heat treatments in H_2 induce major transformations of the hemispherically shaped catalyst. A polyhedral morphology emerges and is characterized by the occurrence of large areas of (001) top and {111}/{011} side planes, in agreement with predictions of equilibrium thermodynamics.[22] A thin rim of stepped planes is seen to separate these low Miller index planes from each other. In such polyhedral morphologies, a low concentration of step sites is present and electron emission is found to be strongest from {113} facets. After preconditioning, acetylene (purity >99.1%) is dynamically added to the hydrogen atmosphere while continuously imaging in FEM. After ~11 s, the equilibrium shape of the Ni catalyst undergoes another significant reconstruction.[23] In particular, this transformation proceeds *via* the shrinking of the central (001) pole and the {111} planes surrounding it. Concomitantly, an extension of the stepped rim between these planes is observed (*i.e.*, the number density of steps is increased). Again, the {113} planes of the <100> zone appear to be the brightest in FEM. The salient

features of the final morphology are depicted in Figure 2c. Since acetylene adsorbs dissociatively at 873 K, our experiments suggest that adsorbed C atoms induce the formation of step sites. The considerable extension of the {113} planes is also in accordance with preferential adsorption of carbon with fivefold coordination at Ni step sites.[3] At the end of the process, a bright pattern appears on the reconstructed Ni crystal (not shown in the movie). The brightness and, consequently, the corresponding field emission current increase exponentially with time and eventually lead to the fracture of the Ni specimen. Such a situation can be easily explained with the growth of a graphitic material,[24,25] inducing a strong decrease of the work function of the tip. We note that under "softer" conditions ($T = 723$ K, using ethanol instead of acetylene), the brightness appears selectively on the extended and C-enriched stepped crystal planes and slowly invades the surface.[26] These planes can thus be associated with preferential graphene nucleation sites while serving as C feedstock during growth.

Since the number density of step sites on an overall polyhedral nanosized Ni crystal is relatively low, the dominating part of the incoming acetylene molecules initially hits atomically flat terrace regions. After dissociative chemisorption, a directional diffusion process of surface carbon to step sites will take place. While this process is too fast to be followed experimentally, it is accessible to tight-binding (TB) Monte Carlo (MC) simulations, which have been performed using a stepped Ni surface. Such studies also allow visualizing C aggregation and, ultimately, graphene sheet formation. In the present model,[10,26] a minimal basis, including s and p electrons of C and d electrons of Ni, is required to obtain a transferable TB model of the C−C, Ni−Ni, and Ni−C interactions applicable to binary systems. This TB model is then implemented in a Monte Carlo code using either a canonical or grand canonical algorithm with fixed volume, temperature, number of Ni atoms, and C chemical potential μ_C.[27] The full structure, including C and Ni atoms, was relaxed *via* standard MC displacement steps. Our simulations were performed at fixed temperature (1000 K) with a chemical potential referring to a fictitious ideal atomic C gas,[28] varying between −6.00 and −4.75 eV/atom (by steps of 0.20 eV/atom) on a Ni(111) surface presenting a single (111) oriented step edge. At low chemical potentials ($\mu_C < -5.9$ eV/atom), C atoms land on the surface and tend to diffuse toward step sites. Some C dimers or trimers are formed in the vicinity of the step edge, although no real C structure is observed yet. Interestingly, the time-resolved chemical probing experiments, which will be described below, demonstrate the occurrence of such short-length carbon polymers as C_n and NiC_n species field evaporating in ionic form. Turning now to simulation studies at high chemical potentials ($\mu_C > -5.50$ eV/atom), by contrast, a disordered and dense amorphous

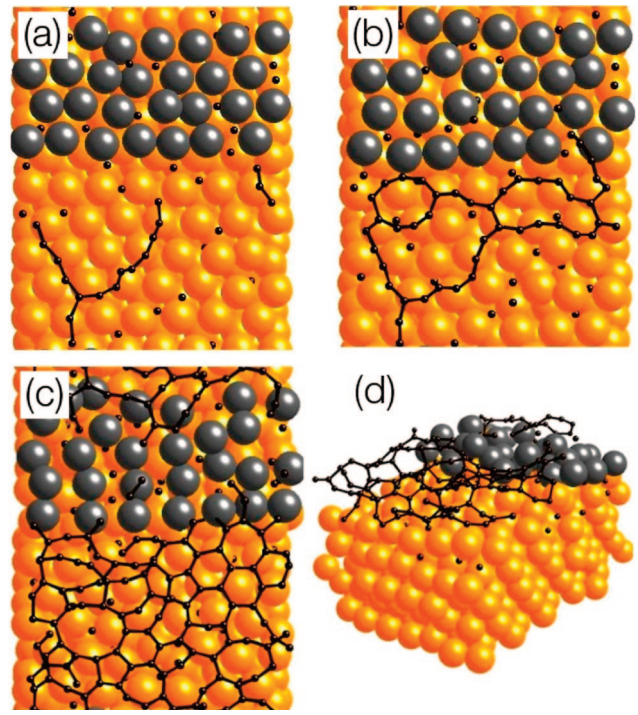

Figure 3. Nucleation and growth sequences of a graphene layer in the vicinity of a step edge in a Ni(111) surface at 1000 K. During the course of the TBMC simulation ($\mu_C = -5.80$ eV/atom), the adsorption of C is observed preferentially at the step edge leading to linear (a) and connected (b) atomic structures to a defective graphene-like sheet (top (c) and side (d) views). Ni atoms are displayed by big orange and gray (step) spheres, while C atoms are shown in black balls-and-sticks representation.

C layer is formed, extending over the entire Ni surface. However, when $\mu_C \in [-5.80; -5.70]$ eV/atom, a sp^2-like structure starts nucleating at the Ni step edge (Figure 3). At the very beginning of the simulation, C atoms land predominantly on the flat terraces of the Ni surface, do not diffuse toward step edges, but tend to form short chains (Figure 3a). For $\mu_C = -5.80$ eV/atom, the number of incoming C atoms is large. They stabilize at the surface by forming C−C bonds with the growing chains interacting strongly with the step edge to create C rings (Figure 3b). Other chains are likewise formed in the vicinity of the step edge which acts as a nucleation center to grow the sp^2-hybridized C layer (Figure 3c,d). As compared to a perfect graphene sheet, our C layer contains a large number of defects which, however, have a very low probability to heal out, due to the short time scale sampled in our simulations. Nevertheless, for specific μ_C conditions, our TBMC model predicts the preferential trapping of C atoms at step edges of Ni surfaces and the formation of a defective graphene-based C layer.

In another experimental setup that combines FEM/FIM and atom-probe techniques, a surface chemical analysis of about 400 atomic surface sites (comprising the (113) plane)) was performed during the ongoing acetylene decomposition/reaction with the Ni crystal. Short field pulses of $F \leq +15$ V/nm at variable fre-

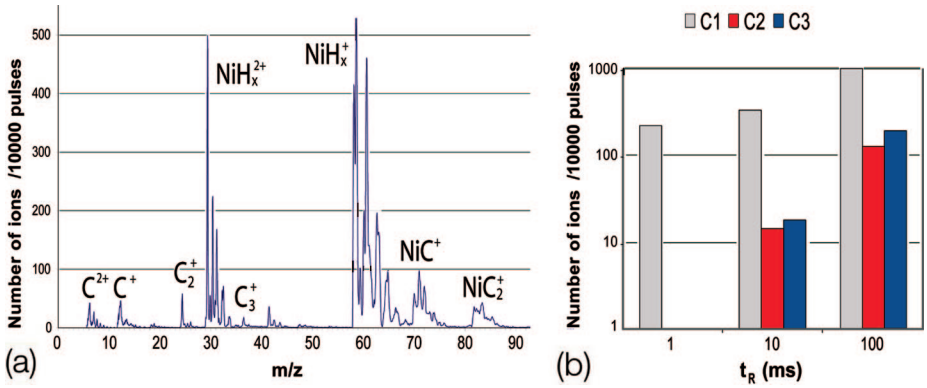

Figure 4. (a) Mass spectrum obtained when exposing a Ni tip to acetylene (T = 723 K, p = 10^{-3} Pa, 10 ms between each pulse, 10^5 pulses, $F \sim$ 10 V/nm). The size of the monitored area containing the (113) plane comprises ~400 atomic Ni atoms. The mass resolution is limited since the ions move in the time-dependent electric field of the pulses (width ~100 ns). While the presence of NiH_x^+ species is assured, the possible existence of CH_y^+ species can only be proven by applying more rigorous time-focusing devices. (b) C_1, C_2, and C_3 intensities as a function of the reaction time t_R (T = 623 K, $p(C_2H_2)$ = 10^{-3} Pa, $F \sim$ 10 V/nm).

quency were applied to cause ionic field desorption and evaporation of surface species. In this experiment, the temperature of the Ni sample was reduced to 723 K in order to accurately control the rate of Ni ionic removal due to field pulses. Figure 4a presents a typical mass spectrum related to field desorption/evaporation. Besides NiH_x (x = 0,1), NiC_n species (n = 1,2) and C_1 to C_3 species (occasionally C_4, as well) are detected with various intensities. While the occurrence of NiC_n ions demonstrates the field-induced removal of carbon atoms along with Ni from steps/kinks, the origin of C_{1-4} must be different. This is suggested by time-dependent measurements which have been performed at somewhat lower temperature, 623 K, to slow down the reaction.

As illustrated in Figure 4b, the C spectrum is dominated by C_1 for a reaction time (t_R) of 1 ms. C_2 and C_3 species are obviously absent at this short time. Increasing t_R to 10 ms causes both C_2 and C_3 to appear in considerable amounts. The fairly distinct time dependence of $C_{2,3}$ as compared to C_1 excludes the possibility of field-induced processes to be responsible for their formation. A reaction process of higher order kinetics (*i.e.*, rate $\sim \Phi^n$ with $n > 1$ (Φ = coverage)) must be in operation to explain the drastic increase of $C_{2,3}$ ionic intensities between 1 and 10 ms. Later on, for 10 ms $\leq t_R \leq$ 100 ms, the $C_{2,3}$ amounts increase proportionally with time. Since the number of ions per pulse is a measure of the surface coverage, Φ, in the probed area of the Ni crystal surface, this is equivalent to a constant formation rate in this time range. By contrast, the C_1 overall time dependence is much weaker so that field fragmentation or association processes cannot be made responsible for C_{2-4} detection. These latter species are thus assumed to reflect their parent analogues formed from a C_1 unity at the Ni surface (or beneath, see below) within several milliseconds at 623 K.

In order to investigate theoretically the stability of carbon fragments (C_n) in the vicinity of the catalytic surface, TBMC simulations are performed on a Ni slab (8 atomic layers; 256 atoms) presenting a (111) surface in a supercell geometry (vacuum region = 20 Å). Both temperature and μ_C are fixed to 1000 K and −6.00 eV/atom, respectively. During the course of the simulation, the adsorption of C atoms start at the crystal surface (landing site). Subsequently, they diffuse to interstitial sites between Ni layers to occupy subsurface position, leading to an important local distortion of the Ni crystal. A strong tendency to form C−C bonds in subsurface positions is observed. The C−C bond length is roughly 1.9 Å, suggesting the formation of C_2 close to the surface, as illustrated in Figure 5a.

This situation corresponds to the saturation of the surface layers of the Ni crystal with C, as suggested in previous growth models.[6,12]

Static TB calculations allow us to predict the stability of these C_2 in subsurface position. The dissolution energy (E_{dis}) of two C atoms separated by a certain distance and located at different depths from the Ni slab surface is defined as $E_{dis} = [E_{C+Ni} - (E_{Ni} + 2E_C)]/2$, where E_{C+Ni} and E_{Ni} represent the total energies of the Ni slab containing two C atoms and the clean ideal Ni slab. E_C is the total energy per atom of a

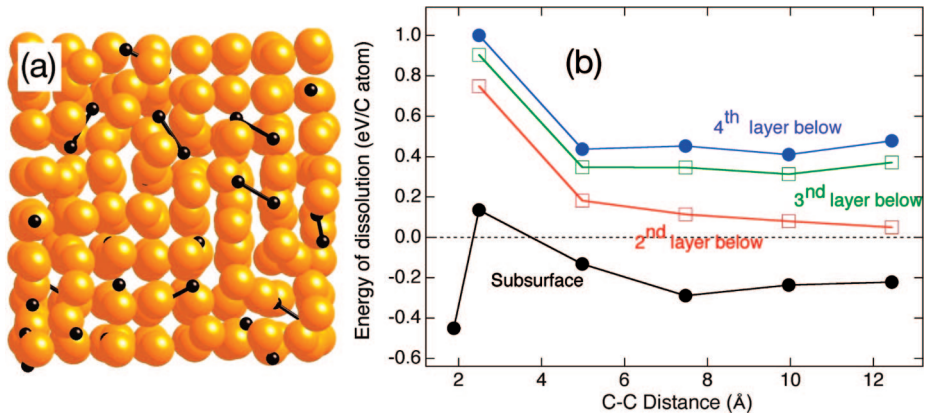

Figure 5. (a) Typical top views of Ni−C structures at 1000 K with low chemical potential for C (μ_C = −6.0 eV/atom). Ni and C atoms are displayed as big orange and small black spheres, respectively. (b) Energy of dissolution of a C dimer in a Ni (111) slab for different C−C distances and at various layer positions with respect to the particle surface. The stability of C dimers (represented by two connected black spheres in (a)) is predicted for the subsurface position.

graphene sheet. All energies are calculated at 0 K on fully relaxed atomic configurations using a larger (111) oriented Ni slab (900 atoms) to take into account long-range elastic effects imposed by the structural relaxation around the C_2. The dissolution energy of a C atom in a bulk octahedral interstitial site is positive (endothermic process) by +0.40 eV within our TB model (very close to the +0.43 eV value determined experimentally).[29] Indeed, an interstitial C atom induces local strain and distortions of the surrounding Ni lattice, contrary to the subsurface position where larger local relaxations are allowed.[26,30] Then, two C atoms have been placed at two different interstitial octahedral sites separated by a specific distance for different depths inside the slab (Figure 5b). The process is found exothermic (endothermic) in subsurface position (deeper in the slab). Approaching the two interstitial C atoms always induces an energy increase due to long-range elastic effects, except in the subsurface position for a very small C−C distance (~1.9 Å). In that case, the presence of C atoms in two nearest-neighboring octahedral sites is particularly favored by the Ni surface which relaxes completely, allowing the formation of C_2 with a strong covalent bond. This situation is not observed for positions deeper inside the slab (Figure 5b).

In summary, the present FEM/FIM experiments suggest that C atoms induce step edge formation on polyhedrally reshaped Ni crystals. Combined *in situ* observations and theoretical simulations illustrate the key role that these carbon-enriched step edges play as nucleation sites for C aggregation and graphene sheet formation. At high adsorption rates, our model predicts the formation of sp^2 C layers starting from the step edge. Time-resolved atom-probe measurements with nanoscale lateral resolution show C_2 and C_3 species to form from C_1 units. This step is slow and of higher kinetic order. Simulations reveal that C_2 species may even be formed in subsurface interstitial sites due to local strain effects associated with the dissolution of C in the Ni particle. The presence of C atoms in subsurface positions has previously been suggested to anchor the nanotube during nucleation.[31] Our combined experimental and theoretical approach thus provides new insight into the early stages of CNT nucleation on a single nanosized Ni catalyst particle.

METHODS

In a first setup of the present study, video-field electron and field ion microscopy (FEM/FIM) are used to image the surface structure of an either clean or adsorbate-covered Ni catalyst conditioned as a single nanosized 3D particle ("field emitter tip") with a hemispherical shape. In a second setup, the same microscopy tools are combined with an "atom-probe" analysis,[33,34] which allows local chemical probing of areas ultimately containing a few Ni atoms of a single nanofacet. Both instrumentations can be operated under *in situ* reaction conditions. In order to investigate the reaction kinetics between single carbon atoms, short field pulses of variable amplitude and repetition frequency are applied under continuous supply of the gaseous reactant. Field pulses lead to the ionic desorption of the adsorbed layer. Respective ions are injected into a time-of-flight mass spectrometer. If the pulse amplitude (*i.e.*, the respective field strength) is high enough, the adsorbed layer is quantitatively removed and the individual ion intensities reflect the surface coverage of the respective species. Varying the repetition frequency, that is, the reaction time between any two pulses, then allows monitoring of the reaction kinetics. Probed surface areas are adjustable and range from the equivalent of a few surface sites of a well-defined nanofacet up to ~400 sites. For kinetic measurements, as those presented here, the upper limit is preferred in order to comply with the need for statistically significant ion intensities at short reaction times. Figure 1b also shows that a steady electric field, F_R, can be maintained while pulsing. In fact, F_R can be varied from the onset of field electron emission to the occurrence of field evaporation (the removal of lattice atoms as ions) at reversed polarity, thus revealing the influence of the electric field on the reaction processes. A clear-cut differentiation between field-induced processes and truly chemical reaction kinetics is provided by following the time dependence of individual ion intensities.

Structural changes and morphological reshaping of Ni field emitter crystals are studied by FEM ($F \leq -3$ V/nm). Step structures remain stable when switching to FIM conditions ($F \sim +35$ V/nm) in the absence of gaseous reactants. Videos are acquired with a high-dynamic range camera at a frame rate of 50 images/s.

Ni tips are electrochemically etched from a high purity wire (Ø ~ 0.1 mm) in diluted HCl (0.5 mol/L). Tip radii of curvature are estimated between 6 and 15 nm. Samples are characterized by FIM. Cycles of thermal annealing, Ne^+ or Ar^+ sputtering, and field evaporation are used to clean the tips before using them in reaction studies. The tip can be heated resistively by passing a current through a tungsten loop onto which it is mounted. Temperatures can then be accurately controlled between 50 and ~1000 K.

In the tight-binding model presented in the theoretical part, a minimal basis, included s and p electrons of C and d electrons of Ni, is required to obtain a transferable TB model of the C−C, Ni−Ni, and Ni−C interactions applicable to binary systems. We use a moment-recursion technique at the level of a fourth moment approximation in order to determine the band energy. Actually, this TB approximation provides an efficient tool to calculate the bonding energies in the Ni−C system where total energies are obtained by adding empirical repulsive terms. For C−C interactions, the tight-binding parameters have been fitted in order to reproduce accurately the competition between sp, sp^2, and sp^3 atomic arrangements. This approach is especially adapted to model curvature in carbon nanostructures. For Ni−Ni interactions, the tight-binding parameters have been fitted on fcc bulk nickel (lattice parameter, cohesive energy, elastic moduli measured experimentally). The crucial point of our tight-binding model is the derivation of Ni−C interactions. Indeed, the corresponding parameters have been constructed using various electronic and structural properties of transition metal carbides, such as the cohesive energy, equilibrium lattice parameter, bulk modulus and enthalpy of formation. Various carbides have been considered to test and improve our model, as described in ref 35. This approach, both simple and accurate, is then implemented in a Monte Carlo code using either a canonical or a grand canonical algorithm with fixed volume, temperature, number of Ni atoms, and C chemical potential μ_C.[27] Applications of this model to surface segregation of carbon and to the catalytic nucleation of carbon caps have already been presented elsewhere.[8,10,26]

Acknowledgment. M.M. and J.-C.C. acknowledge the Fonds de la Recherche Scientifique of Belgium (FRS-FNRS) for financial

support. Parts of this work are also directly connected to the Belgian Program on Interuniversity Attraction Poles (PAI6) on "Quantum Effects in Clusters and Nanowires", to the two ARC entitled: "Hybrid metal/organic nanosystems" and "Phénomènes non linéaires et stochastiques en nanosciences: transport et reaction hors d'équilibre" sponsored by the Communauté Française de Belgique and to the NANOQUANTA and FAME European Networks of Excellence.

Supporting Information Available: Movie 1: Field emission microscopy video presenting the reshaping of a Ni crystal exposed to acetylene at 873 K, $p = 10^{-4}$ Pa. The movie starts with the equilibrated and facetted crystal at 873 K and 10^{-4} Pa in H_2. Acetylene is introduced in the chamber after 1.5 s. Movie 2: Field emission microscopy video showing the nucleation of graphitic carbon during exposure of a Ni crystal to C_2H_5OH at 10^{-4} Pa and 723 K. The movie starts 10 s after having introduced ethanol in the chamber. The initial carbide formation is thus not included. This material is available free of charge *via* the Internet at http://pubs.acs.org.

REFERENCES AND NOTES

1. *Carbon Nanotubes, Advanced Topics in the Synthesis, Structure, Properties and Applications (Topics in Applied Physics)*; Jorio, A., Dresselhaus, G., Dresselhaus, M. S., Eds.; Springer-Verlag: Berlin, Heidelberg, 2008; Vol. 111, pp 1−720.
2. Hofmann, S.; Csányi, G.; Ferrari, A. C.; Payne, M. C.; Robertson, J. Surface Diffusion: The Low Activation Energy Path for Nanotube Growth. *Phys. Rev. Lett.* **2005**, *95*, 036101.
3. Abild-Pedersen, F.; Nørskov, J. K.; Rostrup-Nielsen, J. R.; Sehested, J.; Helveg, S. Mechanisms for Catalytic Carbon Nanofiber Growth Studied by *Ab Initio* Density Functional Theory Calculations. *Phys. Rev. B* **2006**, *73*, 115419.
4. Helveg, S.; López-Cartes, C.; Sehested, J.; Hansen, P. L.; Clausen, B. S.; Rostrup-Nielsen, J. R.; Abild-Pedersen, F.; Nørskov, J. K. Atomic-Scale Imaging of Carbon Nanofibre Growth. *Nature* **2004**, *427*, 426–429.
5. Charlier, J.-C.; De Vita, A.; Blase, X.; Car, R. Microscopic Growth Mechanisms for Carbon Nanotubes. *Science* **1997**, *275*, 647–649.
6. Gavillet, J.; Loiseau, A.; Journet, C.; Willaime, F.; Ducastelle, F.; Charlier, J.-C. Root-Growth Mechanism for Single-Wall Carbon Nanotubes. *Phys. Rev. Lett.* **2001**, *87*, 275504.
7. Raty, J.-Y.; Gygi, F.; Galli, G. Growth of Carbon Nanotubes on Metal Nanoparticles: A Microscopic Mechanism from *Ab Initio* Molecular Dynamics Simulations. *Phys. Rev. Lett.* **2005**, *95*, 096103.
8. Charlier, J.-C.; Amara, H.; Lambin, P. Catalytically Assisted Tip Growth Mechanism for Single-Wall Carbon Nanotubes. *ACS Nano* **2007**, *1*, 202–207.
9. Ding, F.; Rosén, A.; Bolton, K. Molecular Dynamics Study of the Catalyst Particle Size Dependence on Carbon Nanotube Growth. *J. Chem. Phys.* **2004**, *121*, 2775–2779.
10. Amara, H.; Bichara, C.; Ducastelle, F. Understanding the Nucleation Mechanisms of Carbon Nanotubes in Catalytic Chemical Vapor Deposition. *Phys. Rev. Lett.* **2008**, *100*, 056105.
11. Baker, R. T. K.; Barber, M. A.; Harris, P. S.; Feates, F. S.; Waite, R. J. Nucleation and Growth of Carbon Deposits from the Nickel Catalyzed Decomposition of Acetylene. *J. Catal.* **1972**, *26*, 51–62.
12. Lin, M.; Tan, J. P. Y.; Boothroyd, C.; Loh, K. P.; Tok, E. S.; Foo, Y.-L. Direct Observation of Single-Walled Carbon Nanotube Growth at the Atomistic Scale. *Nano Lett.* **2006**, *6*, 449–452.
13. Hofmann, S.; Sharma, R.; Ducati, C.; Du, G.; Mattevi, C.; Cepek, C.; Cantoro, M.; Pisana, S.; Parvez, A.; Cervantes-Sodi, F.; Ferrari, A. C.; Dunin-Borkowski, R.; Lizzit, S.; Petaccia, L.; Goldoni, A.; Robertson, J. *In situ* Observations of Catalyst Dynamics during Surface-Bound Carbon Nanotube Nucleation. *Nano Lett.* **2007**, *7*, 602–608.
14. Mattevi, C.; Hofmann, S.; Cantoro, M.; Ferrari, A. C.; Robertson, J.; Castellarin-Cudia, C.; Dolafi, S.; Goldoni, A.; Cepek, C. Surface-Bound Chemical Vapour Deposition of Carbon Nanotubes: *In situ* Study of Catalyst Activation. *Physica E* **2008**, *40*, 2238–2242.
15. Jin, C.; Suenaga, K.; Iijima, S. How Does a Carbon Nanotube Grow? An *In Situ* Investigation on the Cap Evolution. *ACS Nano* **2008**, *2*, 1275–1279.
16. Yoshida, H.; Takeda, S.; Uchiyama, T.; Kohno, H.; Homma, Y. Atomic-Scale *In-situ* Observation of Carbon Nanotube Growth from Solid State Iron Carbide Nanoparticles. *Nano Lett.* **2008**, *8*, 2082–2086.
17. Vang, R. T.; Honkala, K.; Dahl, S.; Vestergaard, E. K.; Schnadt, J.; Lægsgaard, E.; Clausen, B. J.; Nørskov, J. K.; Besenbacher, F. Ethylene Dissociation on Flat and Stepped Ni(111): A Combined STM and DFT Study. *Surf. Sci.* **2006**, *600*, 66–77.
18. Klink, C.; Olesen, L.; Besenbacher, F.; Stensgaard, I.; Laegsgaard, E.; Lang, N. D. Interaction of C with Ni(100): Atom-Resolved Studies of the "Clock" Reconstruction. *Phys. Rev. Lett.* **1993**, *71*, 4350–4353.
19. Klink, C.; Stensgaard, I.; Besenbacher, F.; Laegsgaard, E. An STM Study of Carbon-Induced Structures on Ni(111): Evidence for a Carbidic-Phase Clock Reconstruction. *Surf. Sci.* **1995**, *342*, 250–260.
20. Klink, C.; Stensgaard, I.; Besenbacher, F.; Laegsgaard, E. Carbidic Carbon on Ni(110): An STM Study. *Surf. Sci.* **1996**, *360*, 171–179.
21. Nakano, H.; Nakamura, J. Carbide-Induced Reconstruction Initiated at Step Edges on Ni(111). *Surf. Sci.* **2001**, *482−485*, 341–345.
22. Herring, C. *Structure and Properties of Solid Surfaces*; Gomer, R., Smith, C. S., Eds.; Chicago University Press: Chicago, IL, 1953; pp 5−81.
23. See Supporting Information (Movie 1 and Movie 2, respectively).
24. Czerwosz, E.; Dluzewski, P.; Kutner, T.; Stacewicz, T. Photoelectric Work Function Studies of Carbonaceous Films Containing Ni Nanocrystals. *Thin Solid Films* **2003**, *423*, 161–168.
25. Hwu, H. H.; Fruhberger, B.; Chen, J. G. Different Modification Effects of Carbidic and Graphitic Carbon on Ni Surfaces. *J. Catal.* **2004**, *221*, 170–177.
26. Amara, H.; Bichara, C.; Ducastelle, F. Formation of Carbon Nanostructures on Nickel Surfaces: A Tight-Binding Grand Canonical Monte Carlo Study. *Phys. Rev. B* **2006**, *73*, 113404.
27. Frenkel, D.; Smit, B. *Understanding Computer Simulation*; Academic Press: London, 1996.
28. The values of μ_C are chosen to be close to cohesive energies of carbon phases (*e.g.*, −7.41 eV/atom for graphene).
29. Shelton, J. C.; Patil, H. R.; Blakely, J. M. Equilibrium Segregation of Carbon to a Nickel (111) Surface: A Surface Phase Transition. *Surf. Sci.* **1974**, *43*, 493–520.
30. Klinke, D. J., II; Wilke, S.; Broadbelt, L. J. A Theoretical Study of Carbon Chemisorption on Ni(111) and Co(0001) Surfaces. *J. Catal.* **1998**, *178*, 540–554.
31. Rodríguez-Manzo, J. A.; Terrones, M.; Terrones, H.; Kroto, H. W.; Sun, L.; Banhart, F. *In-situ* Nucleation of Carbon Nanotubes by the Injection of Carbon Atoms into Metal Particles. *Nat. Nanotechnol.* **2007**, *2*, 307–311.
32. Nakano, H.; Ogawa, J.; Nakamura, J. Growth Mode of Carbide from C_2H_4 or CO on Ni(111). *Surf. Sci.* **2002**, *514*, 256–260.
33. Müller, E. W.; Tsong, T. T. *Field Ion Microscopy, Principles and Applications*; Elsevier: New York, 1969.
34. Kruse, N.; Visart de Bocarmé, T. In *Handbook of Heterogeneous Catalysis*; Ertl, G., Knözinger, H., Schüth, F., Weitkamp, J., Eds.; Wiley-VCH: Weinheim, Germany, 2008; pp 870−895.
35. Amara, H.; Roussel, J.-M.; Bichara, C.; Gaspard, J.-P.; Ducastelle, F. Tight-Binding Potential for Atomistic Simulations of Carbon Interacting with Transition Metals: Application to the Ni−C System. *Phys. Rev. B* **2009**, *79*, 014109.